First-Principles Study of Carbon Monoxide Oxidation on Ag(111) in Presence of Subsurface Oxygen and Stepped Ag(221)

Hai-Yan Su,[†,‡,§] Zhenhua Zeng,[†,‡,§] Xin-He Bao,*,[†] and Wei-Xue Li*,[†,‡]

State Key Laboratory of Catalysis and Center for Theoretical and Computational Chemistry, Dalian Institute of Chemical Physics, Chinese Academy of Sciences, Dalian, 116023, China, and Graduate School of the Chinese Academy of Sciences, Beijing, 100039, China

The role of subsurface oxygen in Ag(111) and the step edge of vicinal Ag(221) on CO oxidation were studied by using density functional theory calculations. For high oxygen coverage, the formation of subsurface oxygen is not only energetically favorable but also kinetically likely. CO oxidation with on-surface atomic oxygen is facile with a barrier of about 0.16 eV, whereas the reaction with subsurface oxygen is hindered because of the significant barrier for diffusion of the subsurface oxygen to the surface from the subsurface region. It is found that the adsorption of molecules (CO, atomic O and O_2) is stabilized in the presence of subsurface oxygen, and surface reactivity is enhanced. An energetically favorable reaction pathway for CO oxidation with O_2 is identified, with a reaction barrier of 0.23 eV via a unique four-center $O_2 \cdots CO$ intermediate. A catalytic cycle for CO oxidation on Ag(111) in the presence of subsurface oxygen is proposed. On Ag(221) surfaces, our calculations show that both the adsorption of the reactants and O_2 dissociation, with a calculated barrier of 0.42 eV compared to 0.95 eV for the clean Ag(111), are promoted significantly at the step edge, and the reactivity for CO oxidation is improved accordingly.

1. Introduction

As one of the unique partial oxidation catalysts for industrial reactions, such as methanol to formaldehyde and ethylene epoxidation, the interaction between silver and oxygen has been studied extensively, both experimentally and theoretically.[1−35] Activation of silver catalysts and the formation of various distinct oxygen species are thought to be crucial for the activity and selectivity of silver catalyzed reactions. So far, various oxygen species, different in terms of their functionalities (partial and full oxidation) and/or geometrical locations (on-surface, subsurface, and bulk-dissolution) have been proposed. Among them, the interactions between oxygen and Ag, for example, O_2 activation, oxygen-induced reconstruction, and the formation of subsurface oxygen have received great attention.[1,2]

To activate bulk silver catalysts and O_2 molecules forming active oxygen species, severe pretreatment of catalysts at elevated temperatures and high pressures (typically 780 K and atmospheric pressure) are required.[3] However, the activation of the silver catalysts and the formation of subsurface oxygen can be facilitated by decreasing the size of silver catalysts down to the nanoscale.[4,5] In this work, it was found that the activated silver nanoparticles have high activity and selectivity for the reactions such as oxidative coupling of methane and partial oxidation of methanol to formaldehyde, and high activity was seen for complete CO oxidation at room temperature (RT). Size dependence of the activity was also reported by Kim and co-workers by using X-ray photoemission spectroscopy (XPS).[6,7] Compared to the oxygen uptake by larger particles and bulk-like Ag, they found that oxygen uptake by the smaller Ag nanoparticles is significantly higher. Two distinct oxygen species

in silver nanoparticles were identified, with either Ag_2O and/or AgO being active for CO oxidation at RT. For activated silver particles, both of on-surface and subsurface oxygen, were proposed to be the active species for CO oxidation.[8,9] In addition, CO oxidation with superoxide has been proposed in surface-science studies on Ag(110) surface.[11−14]

To rationalize these experimental findings, a mechanistic study of silver catalysts upon O_2 activation, by considering the formation of subsurface oxygen and the effect of the particle sizes on well-defined Ag(111) and vicinal surfaces, would be necessary. In the past, various oxygen species (on-surface oxygen, subsurface oxygen, and bulk dissolved oxygen), surface reconstructions, and the formation of surface oxides and bulk oxide on single crystalline surface have been studied extensively both experimentally and theoretically at a wide range of temperatures and oxygen partial pressures, providing a comprehensive picture of oxygen and silver interactions.[15−25] Corresponding thermodynamic phase diagrams based on density functional theory (DFT) calculations have been constructed.[15,19] Although previously proposed O—Ag—O trilayer surface oxide model was subsequently shown to be a surface reconstruction with the same periodicity and the same number of oxygen atoms by Schnadt et al.[21] and Schmid et al.,[22] the phase diagram was only affected slightly because of their similar energetics. Klust and Madix studied the reduction of $p(4 \times 4)$ reconstruction surface with CO at RT by using scanning tunneling microscopy.[25] They found that the reconstructed $p(4 \times 4)$ surface is not reactive. Instead, the boundary between $p(4 \times 4)$ and clean Ag(111) is responsible for the source of the reactive oxygen. The effect of subsurface oxygen on the reactivity of Ag(111) was addressed by Mavrikakis and co-workers by using DFT calculations. Their calculations indicate that subsurface oxygen may facilitate the dissociation barriers of O_2 and NO,[26] whereas ethylene epoxidation elimination from surface oxametallacyles becomes demanding because of the presence of subsurface

* Corresponding authors. E-mail: wxli@dicp.ac.cn and xhbao@dicp.ac.cn.
† State Key Laboratory of Catalysis, Chinese Academy of Sciences.
‡ Center for Theoretical and Computational Chemistry, Chinese Academy of Sciences.
§ Graduate School of the Chinese Academy of Sciences.

oxygen.[27] Recently, by using in situ surface X-ray diffraction at one bar and 773 K, Stierle and co-workers showed that a $p(7 \times 7)$ O—Ag—O trilayer surface oxide and bulk oxide Ag_2O in $(\bar{1}\bar{1}\bar{1})$ orientation exhibit similar honeycomb symmetry, which coexists with a $p(4 \times 4)$ reconstruction.[28] This study suggested that all these structures may be involved in silver catalyzed reactions under realistic conditions.

To shed light on the catalytic role of subsurface oxygen in CO oxidation on Ag(111) and the effect of the step edge on the Ag(221) surface, we performed a systematic DFT study with emphasis on the formation of subsurface oxygen and its effects on adsorption of reactants (O_2 and CO) and O_2 activation as well as CO oxidation. We find that, at high oxygen coverage, the formation of subsurface oxygen on Ag(111) is not only energetically favorable but also kinetically likely. CO oxidation with on-surface atomic oxygen is a facile process, but the reaction with subsurface oxygen is kinetically hindered because of the significant barrier for diffusion to the surface from the subsurface region. The presence of subsurface oxygen enhances the surface reactivity and stabilizes the adsorbates. An energetically favorable reaction pathway between coadsorbed CO and O_2 molecules via a four-center $O_2 \cdots CO$ intermediate is identified. On stepped Ag(221) surface, we find that O_2 dissociation (the rate limiting step on closed packed Ag(111) surface) at the step edge is facilitated, and the dissociated atomic oxygen reacts quickly with adsorbed CO to form CO_2. The role of the step edge in silver nanoparticles is highlighted. The remainder of the paper is organized as follows. The calculation methods are introduced in Section 2. In Section 3, the formation of subsurface oxygen as well as its effects on the adsorption, dissociation, and CO oxidation are presented. O_2 dissociation and CO oxidation on Ag(221) are discussed in Section 4. Finally, the conclusions are briefly summarized in Section 5.

2. Methods

DFT calculations were performed by using the DACAPO code,[36] in which the ionic cores were described by ultrasoft pseudopotentials. The Kohn—Sham one-electron valence states were expanded in a plane-wave basis set with a kinetic energy cutoff at 340 eV, with the exchange and correlation energies approximated by a generalized gradient functional, GGA-PW91.[37,38] During iterative diagonalization of the Kohn—Sham Hamiltonian, a Fermi population of the Kohn—Sham states ($k_B T$ = 0.1 eV) and Pulay mixing of the resulting electronic density were used to improve the numerical stability. The total energies calculated were then extrapolated to absolute zero.

The Ag(111) surface was represented by a four-layer slab, and the Ag(221) surface was represented by three equivalent (111) layer slabs. Both slabs were separated by seven equivalent layers of vacuum. Adsorption was allowed on the relaxed side of the slab where the induced dipole moments was taken into account by applying a dipole correction.[39] The adsorbates, the top two metal layers of Ag(111), and the topmost metal layer of Ag(221) were optimized until a maximum force of 0.02 eV/Å was obtained. Supercells with a periodicity of (2×3) and (2×2) for Ag(111) and (2×1) for Ag(221) were employed to study adsorption and reactivity at different coverages, and a Monkhorst Pack mesh with a ($4 \times 4 \times 1$) grid was used for k-point sampling in the surface Brillouin zone of the unit cells. For reference, a calculated equilibrium lattice constant of 4.14 Å was obtained for Ag, in good agreement with the experimental value of 4.09 Å[40] and previous calculations,[26] and has been used throughout the present work. Calculated binding energies for H_2 and O_2 molecules in the gas phase were −4.56 and

−5.12 eV, respectively.[41]

The transition states (TSs) of the reactions were searched by constraining the distance between the reactants at various values with a step size of 0.1 Å while relaxing all the other degrees of freedom simultaneously.[42] For the diffusion of oxygen penetration into subsurface regions, the TS corresponds to the O atom in the plane of the surface Ag layer from the on-surface fcc site to the subsurface octahedral or tetrahedral site.[16] We fully relaxed the first two Ag layers, but to stay at the TS, we constrained O to be in the plane of the first Ag(111) layer.

The average adsorption energy per oxygen atom, $E_{ads}(O)$, is calculated according to

$$E_{ads}(O) = [E^{O/Ag} - (E^{Ag} + 0.5 \times N_O E^{O_2})]/N_O$$

where N_O is the total number of oxygen atoms of the adsorbate—substrate system per unit cell, and the total energy of the adsorbate—substrate system, the clean surface (Ag(111) and/or Ag(221)), and the free oxygen molecules are represented by $E^{O/Ag}$, E^{Ag}, and E^{O_2}, respectively. That is, $E^{O/Ag}$ represents the O/Ag system under investigation, which, for example, may involve purely subsurface O or on-surface and subsurface species. The CO adsorption energy, $E_{ads}(CO)$, is defined similarly.

To study the interaction between on-surface and subsurface oxygen, we consider how the stability of on-surface O is affected by subsurface O (and vice versa). To do this, we define a so-called removal energy, $E_{on}^{removal}$, which is the energy required to remove an on-surface O atom into the vacuum. It is given as

$$E_{on}^{removal} = E^{O/Ag} - (E^{O_{sub}/Ag} + 0.5 \times N_O E^{O_2})$$

where $E^{O_{sub}/Ag}$ is the total energy of the reference" system, that is, that containing only (one or more) subsurface O species. $E_{on}^{removal}$ can also be thought of as the adsorption energy of an O atom onto the substrate which contains the subsurface O atoms. An obvious analogous equation holds for the removal energy of a subsurface O atom $E_{sub}^{removal}$

$$E_{sub}^{removal} = E^{O/Ag} - (E^{O_{on}/Ag} + 0.5 \times N_O E^{O_2})$$

where $E^{O_{on}/Ag}$ is the total energy of the reference system, that is, that containing only (one or more) on-surface O species. The adsorption and removal energies are defined such that a positive number indicates that the adsorption is exothermic (stable) with respect to a free O atom and a negative number indicates an endothermic (unstable) reaction.

3. Results

3.1. Oxygen Adsorption and Formation of Subsurface Oxygen. Our earlier calculations[43] show that O_2 molecules bind weakly on Ag(111) with an adsorption energy of −0.16 eV and the barrier for O_2 dissociation (1.03 eV) is significant. These results agree well with previous theoretical calculations[26] and Campbell's experimental findings of a very low sticking coefficient.[33] At low coverage, a dissociated oxygen atom on Ag(111) prefers to adsorb at on-surface fcc hollow sites, and occupation at subsurface interstitial sites is energetically unfavorable because of the significant deformation induced by subsurface oxygen.[15−18] At high coverage, the electrostatic repulsion between adsorbed on-surface oxygen increases, and adsorption on the surface becomes energetically less favorable. At 1/6 ML (see Table 1 and Figure 1a,b), the calculated (dissociative) adsorption energy $E_{ads}(O)$ on the fcc sites is −0.51 eV/O (exothermic), but $E_{ads}(O)$ at subsurface tetrahedral (de-

TABLE 1: Calculated Average Adsorption Energies for Dissociative Oxygen Atoms $E_{ads}(O)$ and CO on Ag(111) as a Function of O Coverage (ML)[a]

θ_{tot}	θ_{on}	θ_{tetra}	$E_{ads}(O)$		$E_{ads}(CO)$
0.00	0.00	0.00			−0.31
1/6	1/6	0.00	−0.51		−0.43
1/6	0.00	1/6	0.12		−0.64
1/4	1/4	0.00	−0.42		−0.44
1/4	0.00	1/4	0.42		−0.70
θ_{tot}	θ_{on}	θ_{tetra}	$E_{ads}(O)$	$E_{on}^{removal}$	$E_{sub}^{removal}$	$E_{ads}(CO)$
1/3	1/6	1/6	−0.37	−0.85	−0.22	−0.48
1/2	1/4	14	−0.35	−1.12	−0.28	−0.22

[a] $E_{on}^{removal}$ and $E_{sub}^{removal}$ are the corresponding removal adsorption energies for O_{on} and O_{tetra}. The unit of energy is eV.
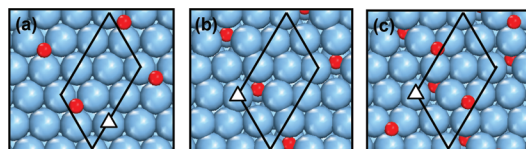

Figure 1. (Color online) Top-view of oxygen adsorption on Ag(111): on-surface oxygen (a) and subsurface tetrahedral oxygen adsorption (b) at coverage of 1/6 ML and adsorption involved both on-surface and subsurface tetrahedral oxygen at total coverage of 1/3 ML (c). The favorable CO adsorption sites (triangle) are indicated. Silver and oxygen atoms are represented by big blue and small red balls, respectively.

Figure 2. (Color online) The potential energy surfaces of oxygen penetration into the subsurface region: (a) from on-surface fcc sites (IS) into subsurface octahedral sites (FS) at coverage of 1/9 ML (adopted from ref 18) and (b) from configuration of Ag(111)-(2 × 3)-2(O_{fcc}+O_{hcp}) (IS) to Ag(111)-(2 × 3)-2(O_{fcc}+O_{tetra}) (FS) at total coverage of 1/3 ML. Corresponding structures are shown schematically in the inset. The barriers for the penetration into the subsurface region, the reversed process, and the reaction energies with ΔE in eV are indicated.

noted by tetra) sites is 0.12 eV/O and endothermic. At $\theta = 1/4$ ML, $E_{ads}(O)$ are −0.42 eV/O (for on-surface fcc oxygen) and 0.42 eV/O (for subsurface tetra oxygen). This means that, at 1/4 ML, oxygen continues to prefer sites on the surface, although the bond strength between oxygen and substrate decreases slightly.

For the formation of subsurface oxygen, penetration of on-surface oxygen into the subsurface region is necessary. Calculated barriers at $\theta = 1/9$ ML are 0.86 and 0.18 eV for the oxygen diffusing to the surface from the subsurface region.[16] From Figure 2a, it is clear that for the low oxygen coverages, the formation of subsurface oxygen is not only energetically unfavorable but also kinetically unstable. When the coverage is higher than 1/4 ML, oxygen starts to penetrate into the subsurface region.[16,17] To simulate this, two oxygen atoms are placed initially at the on-surface fcc and hcp hollow sites in a (2 × 3) supercell (corresponding to a total coverage 1/3 ML), and on-surface fcc oxygen and subsurface tetrahedral oxygen (Figure 1c) from the penetration of on-surface hcp oxygen act as the final states. The incorporated barrier is 0.39 eV, and that for the reverse process is 0.60 eV. In contrast to oxygen incorporation at the low coverage (1/9 ML), which is endothermic (0.68 eV) and kinetically demanding (Figure 2a), the incorporation process at higher coverage (1/3 ML) is exothermic (0.21 eV) and kinetically favorable, as shown in Figure 2b. The calculated (average) adsorption energy for the fcc+tetra configurations formed is −0.37 and −0.35 eV/O when on-surface oxygen and subsurface oxygen are placed in a (2 × 2) supercell (corresponding to a total coverage of 0.5 ML). As noted above, when oxygen atoms are exclusively at on-surface fcc sites and subsurface tetra sites at 1/4 ML, the calculated adsorption energies are −0.42 and 0.42 eV/O, respectively. The structure formed involving both on-surface fcc and subsurface tetrahedral oxygen resembles the O—Me—O trilayer structures, which is a typical structure found in the late transition metal surfaces under oxidizing conditions.[15,19,44−46]

3.2. CO and O$_2$ Adsorption. CO adsorption on Ag(111) with and without the presence of subsurface oxygen is studied in this section. A number of high-symmetry sites are explored,
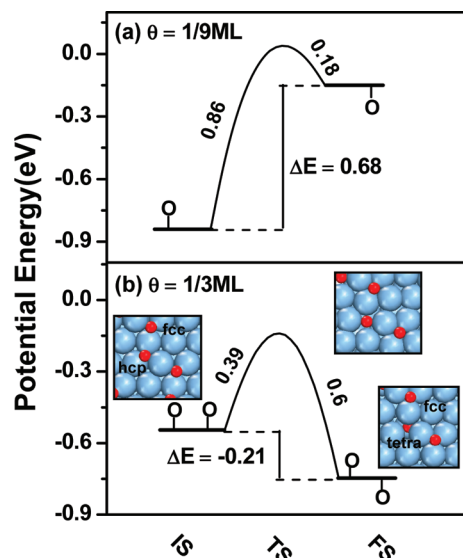
and only energetically favorable configurations are described here. Calculated adsorption energies are listed in Table 1. Compared to CO adsorption on the clean Ag(111)-(2 × 3) surface, which has a binding energy of −0.31 eV (top site), CO adsorption at oxygen precovered (1/6 ML and 1/4 ML) Ag(111) surfaces is enhanced slightly, and calculated adsorption energies are −0.43 and −0.44 eV, respectively. As shown in Figure 1a, CO adsorbs preferentially at top sites with on-surface oxygen atoms nearby not sharing any surface metal atoms. There is no site competition between reactants, but coadsorbed O and CO are close enough to interact through the substrates.

The effect of subsurface oxygen (1/6 ML) on CO adsorption was studied, and the optimized configuration is indicated in Figure 1b: CO adsorbs at the top sites, and the Ag atoms underneath coordinates with subsurface oxygen. Corresponding adsorption energies (Table 1) are −0.64 eV (1/6 ML) and −0.70 eV (1/4 ML). The enhanced binding of CO with respect to the clean Ag(111) substrate comes from the Ag 4d-band upshift (not shown here) of coordinated Ag atoms induced by subsurface oxygen. Similar stabilization can also be seen for oxygen, which can be recognized by calculating the so-called removal energy of on-surface and subsurface oxygen in O_{fcc}—Ag(111)—O_{tetra}
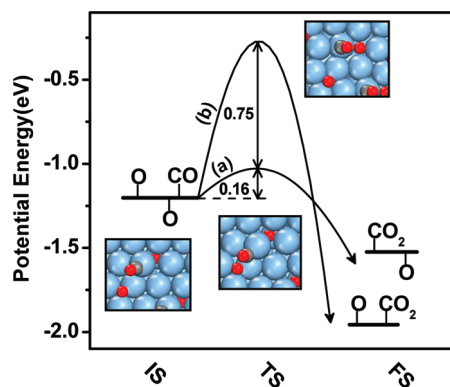
Figure 3. (Color online) The potential energy surfaces of CO oxidation with on-surface oxygen (a) and subsurface tetrahedral oxygen (b) on Ag(111)-(2 × 3)−2(O_{fcc}+O_{tetra}). The initial state (IS) and the TSs identified (CO oxidation with on-surface O_{fcc} for path (a) and oxygen diffusing to the surface from the subsurface region for path (b)) are shown schematically in the inset. Silver, carbon, and oxygen atoms are represented by big blue, small gray, and red balls, respectively.

TABLE 2: Calculated Reaction Barriers E_{act} (in eV) and Important Structural Parameters (in Å) at TSs for CO Oxidation on Ag(111) -(2 × 3) Involved with both On-Surface and Subsurface Oxygen at Total Coverage of 1/3 ML

	E_{act}	d (C—O_{on})	d (C—Ag)	d (O_{on}—Ag)	d (O_{sb}—Ag)
TS(i)	0.16	2.15	2.08	2.13	2.10
TS(ii)	0.91	4.32	2.31	2.21	2.17

trilayer structures. As listed in Table 1, calculated removal energies are $E_{on}^{removal}$ = −0.85 eV and $E_{sub}^{removal}$ = −0.22 eV for the (2 × 3) surface with an overall oxygen coverage of 1/3 ML, and $E_{on}^{removal}$ = −1.12 eV and $E_{sub}^{removal}$ = −0.28 eV for the (2 × 2) surface (1/2 ML).

Molecular (for instance CO and O_2) adsorption on Ag surface involved with both on-surface and subsurface oxygen, O_{fcc}—Ag(111)—O_{tetra}-(2 × 3) trilayer structure are also studied. The most favorable CO adsorption site is shown in Figure 1c, and a corresponding adsorption energy of −0.48 eV is obtained, which is similar to CO adsorption on the oxygen precovered surface. For O_2, the calculated adsorption energy is −0.10 eV, the binding energy of which is slightly weaker than that of O_2 adsorption on the clean Ag(111)-(2 × 3) surface (− 0.16 eV).

3.3. CO Oxidation. In our previous study, we found that clean Ag binds weakly with various adsorbates, which limits its overall reactivity.[43] Accordingly, activation of a silver surface is required. On the O_{fcc}—Ag(111)—O_{tetra} surface, the adsorption energies for CO and O_2 are −0.48 and −0.10 eV, respectively. This shows that CO adsorption on activated O_{fcc}—Ag(111)—O_{tetra} surface is preferential. For CO oxidation on this surface, the following questions should be addressed. First, which oxygen will react with adsorbed CO, on-surface or subsurface oxygen? Second, once on-surface and/or subsurface oxygen is consumed, how may of these active oxygen species will be replenished to close the catalytic cycle?

We first studied CO reaction with on-surface O_{fcc}. The potential energy surface is plotted in Figure 3a (TS given in the inset), and the main structural parameters are listed in Table 2. At the TS, the OC—O_{fcc} bond length is 2.15 Å, and the calculated reaction barrier is 0.16 eV. This is similar to of clean Ag(111) which has a barrier of 0.20 eV.[43] This result shows that the elementary reaction step for CO oxidation with on-surface oxygen is facile and less affected by subsurface oxygen.
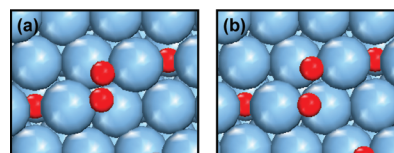

Figure 4. (Color online) Schematic structures of the initial state (a) and TS (b) of O_2 dissociation on Ag(111)-(2 × 3) with presence of subsurface tetrahedral oxygen. Silver and oxygen atoms are represented by big blue and red balls, respectively.

For CO oxidation with subsurface oxygen, subsurface oxygen (O_{tetra}) has to diffuse to the surface from the subsurface region through the close-packed Ag(111) surface. The calculated potential energy surface is plotted in Figure 3b, and the corresponding TS is indicated in the inset. Here, the diffused subsurface oxygen is embedded in the surface Ag layer. The main structural parameters of the TS are given in Table 2, and the calculated barrier is 0.91 eV. Compared to the surface without coadsorbed CO (0.60 eV, Figure 2b), the significant increase of the barrier shows that the presence of coadsorbed CO prevents the diffusion of subsurface oxygen, because both species share common surface metal atoms as indicated in Figure 3. Because the barrier is higher than the adsorption energy of CO (−0.48 eV), CO will desorb from the surface instead of reacting with subsurface oxygen; that is, explicit CO oxidation with subsurface oxygen cannot take place.

Once on-surface oxygen reacts with coadsorbed CO and the CO_2 formed desorbs from the surface, free surface sites on the Ag(111)-(2 × 3) surface in presence of subsurface O_{tetra} are available for O_2 adsorption. A number of high-symmetry sites have been explored, and the most stable structure is shown in Figure 4a. In this structure, every O atom in an O_2 molecule binds with one surface Ag atom, which coordinates linearly with O_{tetra}, forming again a O_{fcc}—Ag—O_{tetra}-like structure. In comparison with O_2 adsorption on the clean Ag(111) surface, which has an adsorption energy of −0.16 eV, the adsorption energy of O_2 on this structure is −0.46 eV. O_2 adsorption is stabilized pronouncedly in the presence of subsurface oxygen. The adsorption energy of an O_2 molecule on Ag surface in the presence of subsurface oxygen is comparable with that of CO on the surface (−0.64 eV), which means that both molecules may adsorb competitively on the surface.

The dissociation of adsorbed O_2 was studied by stretching the O=O bond gradually, and the TS identified is shown in Figure 4b. At the TS, two O atoms adsorb at the bridge sites with an elongated bond length of 2.07 Å. Compared to the bond length of adsorbed O_2 at IS (1.47 Å), the structure identified is a typical late TS. The calculated barrier is 0.83 eV (Figure 5a, solid line, TS1), which is 0.12 eV lower than that of clean Ag(111) (Figure 5a, dash line, TS1). Similar results were reported in ref 26. Though O_2 dissociation is promoted by the presence of subsurface oxygen, the calculated barrier remains too high compared with the adsorption energy of CO. Therefore, the activity for CO oxidation via dissociated atomic oxygen should be low.

In addition to CO oxidation with dissociated atomic O, adsorbed O_2 may react directly with CO to form CO_2. Exactly this was found by our recent calculations on the clean Ag(111) surface in the presence of water[43] and by others on Au surfaces.[47] This was studied further in the present work, and an energetically favorable reaction path has been identified, as shown in Figure 6a. At the initial state, CO adsorbs at the top site and the Ag atom underneath coordinates with subsurface oxygen, whereas O_2 adsorbs at the neighboring bridge-fcc-top site. The corre-
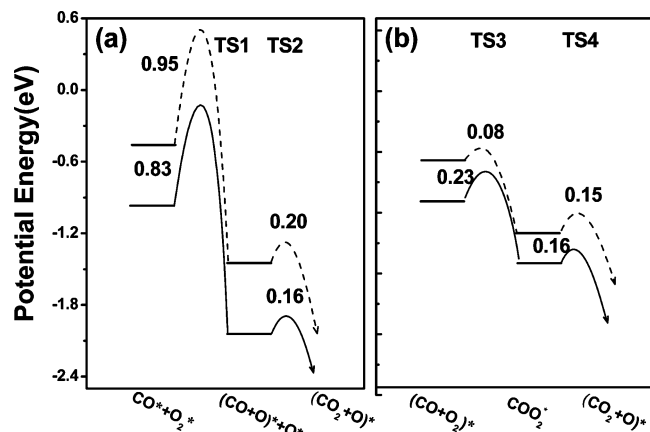
Figure 5. Potential energy surfaces for CO oxidation via atomic oxygen ($O_2 \rightarrow 2O$, $CO + O \rightarrow CO_2$) (a) or molecular oxygen (b) on Ag(111) without (dashed line) and with (solid line) the presence of subsurface oxygen. Calculated barriers are indicated in the figure.
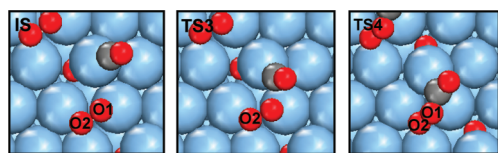

Figure 6. (Color online) The schematic structures (top view) of CO oxidation with O_2 molecule on Ag(111)-(2 × 3) in the presence of subsurface tetrahedral oxygen, as indicated in the potential energy surfaces solid line in Figure 5b. Silver, carbon, and oxygen atoms are represented by big blue, small gray, and red balls, respectively.

TABLE 3: Calculated Total Adsorption Energies E_{coads} and Activation Energies E_{act} and Structural Parameters for CO Oxidation via O_2 Molecules on Ag(111)-(2 × 3) in the Presence of Subsurface Oxygen, as Indicated in Figure 5^a

	energy	d (O1—O2)	d (C—Ag)	d (O_{sb}—Ag)	d (C—O1)
IS	$E_{coads} = -0.91$	1.37	1.99	2.22	3.34
TS1	$E_{act} = 0.23$	1.38	2.05	2.17	2.09
MS	$E_{coads} = -1.41$	1.48	2.09	2.18	1.36
TS2	$E_{act} = 0.16$	1.68	2.11	2.21	1.31

^{a} The Units of Length and Energies are Å and eV, respectively.

sponding removal energies for coadsorbed O_2 and CO are -0.40 and -0.58 eV, respectively. For the reaction between CO and O_2, the O_2 molecule approaches the coadorbed CO, and after a low barrier of 0.23 eV (TS3, Figure 6b), a metastable $O_2 \cdots CO$ intermediate is formed. Stretching the O—O bond of the $O_2 \cdots CO$ complex further to 1.68 Å (other structural parameters are presented in Table 3), the second TS (TS4, Figure 6c) is reached. The calculated barrier is 0.16 eV, and the low barrier comes from the characteristic of the earlier TSs at TS4, in comparison with the O—O bond length 1.37 Å at the initial state. The potential energy surfaces for CO oxidation via O_2 molecules are plotted in Figure 5b. By calculating vibrational frequencies of the metastable $O_2 \cdots CO$ species, we find that compared to the C—O and O—O stretching in the gas phase, there is a significant red shift by ca. 500 and 821 cm^{-1} for O—C stretching and O—O stretching, respectively. This may be used as a fingerprint for verifying the existence of the intermediates experimentally.

3.4. Discussion. Under realistic conditions (elevated temperatures and oxygen partial pressures), a silver surface may reconstruct to $p(4 \times 4)$ and form $p(7 \times 7)$ surface oxide (trilayer) and/or bulk silver oxide.[28] Present DFT calculations show that the interaction between CO/O_2 on the O—Ag(111)—O
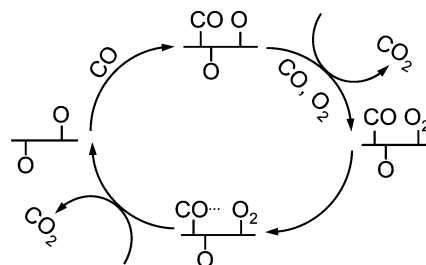
trilayer structure may be enhanced compared with clean Ag(111), and the reactivity of silver surfaces in the presence of subsurface oxygen increases correspondingly.

The overall potential energy surfaces obtained for O_2 dissociation and CO oxidation with atomic oxygen are shown in Figure 5a for clean Ag(111) (dashed line) and the O—Ag(111)—O surface (solid line), respectively. Although subsurface oxygen stabilizes adsorption of O_2 molecules and facilitates O_2 dissociation slightly, the barrier remains considerably higher than that for the adsorption energy of reactants. Thus, the probability that CO oxidation occurs via direct O_2 dissociation on O—Ag(111)—O is not very high.

An energetically favorable reaction pathway for CO oxidation without involving O_2 dissociation explicitly was identified, and the calculated potential energy surface is plotted in Figure 5b (solid line). By forming a four-center $O_2 \cdots CO$ intermediate, the TSs are reached without significant stretching of the O_2 molecules. The calculated overall reaction barrier is 0.23 eV on O—Ag(111)—O, which is lower than the adsorption energy of O_2 (-0.40 eV) and CO (-0.58 eV). This means that on activated O—Ag(111)—O surfaces, not only the adsorption of reactants are enhanced, but also the elementary activity with respect to the CO oxidation is increased. After this, a CO_2 molecule is formed and desorbs from the surface with an atomic O remaining on the surface. This atomic O can be removed quickly by combining with CO by a very low barrier (0.16 eV, as shown above). The catalytic cycle is closed and shown schematically in Figure 7.

We note that the calculated O_2 adsorption energy on a clean Ag(111) is -0.16 eV, which is close to the CO oxidation barrier (0.15 eV) via a similar four-center $O_2 \cdots CO$ intermediate.[43] Nevertheless, the weak adsorption of various reactants on Ag(111) limits its overall reactivity. The stabilization induced by subsurface oxygen found here is crucial. In this context, we note that the enhanced reactivity via the stabilization of the reactants, intermediates, and TSs may be realized by the addition of some water and the formation of the hydrogen bonds in the systems. This was recently found by us[43] on Ag and Au surfaces and by others on Pt[48] and Au.[49]

Our calculations indicate that the Ag surface in the presence of subsurface oxygen is a good catalyst for CO oxidation at low temperatures, which is consistent with recent experimental studies.[4–6] Although the formation of subsurface oxygen requires severe conditions, for example 1 bar and 773 K for bulk silver,[28] it can be formed under modest conditions by decreasing the dimension of the silver catalysts, as found recently by our experiments.[4,5] Reactivity studies on nanosized silver catalysts show that CO may be completely converted to CO_2 at RT. For silver particles (>3 nm) pretreated by atomic oxygen, Kim and co-workers observed two distinct oxygen species from XPS measurements and attributed the treated silver particles to Ag_2O oxide.[6] Interestingly, they find that only one of the oxygen

Figure 7. Catalytic cycle for CO oxidation on Ag surface in the presence subsurface oxygen.

TABLE 4: Calculated Adsorption Energies E_{ads} for CO, O$_2$, and Atomic Oxygen as well as Reaction Barrier for O$_2$ Dissociation and CO Oxidation with Atomic Oxygen at the Step Edge of Ag(221). The Adsorption Sites and Corresponding TSs are indicated in Figure 8^a

	Adsorption Energy
CO	−0.49 (−0.31)
O$_2$	−0.41 (−0.16)
O	−0.80 (−0.51)
	Activation Energy
O$_2 \rightarrow$ 2O	0.42 (0.95)
CO + O $\rightarrow$ CO$_2$	0.24 (0.20)

^{a} The unit of energies is eV, and the numbers given in bracket correspond the results of clean Ag(111).
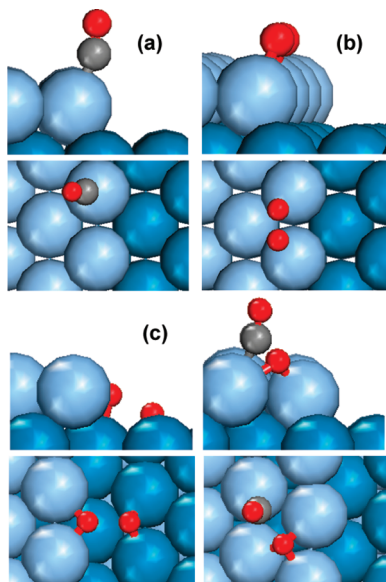

Figure 8. (Color online) Schematic structures for CO (a) and O$_2$ (b) adsorption, and the TSs for O$_2$ dissociation (c) and CO oxidation with atomic oxygen (d) on Ag (221) surface. Silver, carbon, and oxygen atoms are represented by big blue, small gray, and red balls, respectively.

species is active for CO oxidation at RT, whereas the other one is not reactive. This is in line with the present calculations.

4. CO Oxidation on Stepped Ag Surfaces

Small metal nanoparticles are composed of various facets with different orientations, which may facilitate the formation of subsurface oxygen and surface oxide.[50] On the other hand, there is a considerable number of coordinate unsaturated sites (CUS), such as edges and kinks, which are known to be highly active, such as for O$_2$ dissociation.[51] As a result, dissociated atomic oxygen at the step edge may either diffuse into the subsurface region to form subsurface oxygen, act as nucleation site for the oxidation of metal particles, or react with CO to form CO$_2$. Because the local geometry at the step edge and on the various exposed facets is very different from the close-packed surfaces discussed above, the possible reaction pathways for nanocatalysts may be very different. Further, the catalytic activity and selectivity could be modified significantly, as demonstrated by recent DFT calculations.[52,53]

To study the edge effect on silver nanoparticles for CO oxidation, the Ag(221) surface was used as a model system in the present work. CO and O$_2$ adsorption energies at the step edge were calculated, and the results are listed in Table 4.

Calculated CO adsorption at the top site of the step edge (Figure 8a) is −0.49 eV, which is slightly stronger than that for the clean Ag(111) surface (−0.31 eV), as expected. On the other hand, for O$_2$ adsorption, the optimized configuration is shown in Figure 8b, and the corresponding adsorption energy is −0.41 eV, which is much stronger than that for O$_2$ adsorption (−0.16 eV) on the clean Ag(111) surface. The high reactivity for CO and O$_2$ adsorption at the CUS along the step edge can be seen. Enhanced reactivity of the step edge can be seen more clearly from the calculated barrier for O$_2$ dissociation, 0.42 eV, which is significantly lower than that of clean surface (0.95 eV). The low barrier for O$_2$ dissociation comes not only from the electronic effect of the CUS along the step edge but also from the geometric effect for the favorable TSs. As indicated in Figure 8c, the elongated O$_2$ bond of the TS coordinates with five silver atoms (ensemble), and there is no site competition between the dissociating oxygen atoms, which exists however on the perfect Ag(111) surface. Dissociated atomic oxygen reacts with adsorbed CO easily. The TS is plotted schematically in Figure 8d, and the corresponding barrier is 0.24 eV. The enhanced reactivity of the step edge of the silver particles for CO oxidation is thus clearly illustrated.

5. Conclusions

In summary, DFT calculations were used to study CO oxidation on Ag(111) in the presence of subsurface oxygen and stepped Ag(221) surfaces, which are relevant for the silver nanoparticles under elevated temperatures and pressures. Although subsurface oxygen is unstable at low coverage, our calculations show that, at high coverage, formation of subsurface oxygen is not only energetically favorable but also kinetically likely. An increase in reactivity has been found due to the presence of subsurface oxygen and coordinate unsaturated sites along the step edge, which stabilize CO and O$_2$ adsorption. Moreover, a favorable oxidation path between CO and O$_2$ molecules via a four-center intermediate is identified on the silver surface in the presence of subsurface oxygen. On Ag(221), both electronic and geometric effects of the step edge facilitate significantly O$_2$ dissociation, which leads accordingly to a high activity of CO oxidation. The present work indicates that the presence of subsurface oxygen and step edges enhances efficiently the oxidation reactivity of silver catalysts. Because the ability to form subsurface oxygen and the amount of step edges increase with decreasing the silver particle size, the present work indicates that nanosized silver particles may be used as efficient oxidation catalysts at low temperature such as CO oxidation and methanol partial and oxidative methane coupling.[4,5]

References and Notes

(1) Millar, G. J.; Nelson, M. L.; Uwins, P. J. R. *J. Catal.* **1997**, *169*, 143.

(2) Van Veen, A. C.; Hinrichsen, O.; Muhler, M. *J. Catal.* **2002**, *210*, 53.

(3) Bao, X. H.; Muhler, M.; Schedel-Niedrig, T.; Schlögl, R. *Phys. Rev. B* **1996**, *54*, 2249.

(4) Liu, H. Y.; Ma, D.; Bao, X. H. *Chem. Comm.* **2008**, *23*, 2677.

(5) Ma, D.; Sun, J. M.; Miao, S. J.; Liu, H. Y.; Fan, Y. F.; Su, H. Y.; Li, W. X.; Bao X. H. unpublished.

(6) Lim, D. C.; Lopez-Salido, I.; Kim, Y. D. *Surf. Sci.* **2005**, *598*, 96.

8272 *J. Phys. Chem. C, Vol. 113, No. 19, 2009*

Su et al.

(7) Lim, D. C.; Lopez-Salido, I.; Dietsche, R.; Kim, Y. D. *Surf. Sci.* **2007**, *601*, 5635.

(8) Qu, Z. P.; Cheng, M. J.; Huang, W. X.; Bao, X. H. *J. Catal.* **2005**, *229*, 446.

(9) Qu, Z. P.; Huang, W. X.; Cheng, M. J.; Bao, X. H. *J. Phys. Chem. B* **2005**, *109*, 15842.

(10) Chen, L. M.; Ma, D.; Bao, X. H. *J. Phys. Chem. C* **2007**, *111*, 2229.

(11) Burghaus, U.; Vattuone, L.; Gambardella, P.; Rocca, M. *Surf. Sci.* **1997**, *374*, 1.

(12) Burghaus, U.; Conrad, H. *Surf. Sci.* **1996**, *352−354*, 253.

(13) Burghaus, U.; Conrad, H. *Surf. Sci.* **1996**, *364*, 109.

(14) Barth, J. V.; Zambelli, T. *Surf. Sci.* **2002**, *513*, 359.

(15) Li, W. X.; Stampfl, C.; Scheffler, M. *Phys. Rev. Lett.* **2003**, *90*, 256102.

(16) Li, W. X.; Stampfl, C.; Scheffler, M. *Phys. Rev. B* **2003**, *67*, 045408.

(17) Li, W. X.; Stampfl, C.; Scheffler, M. *Phys. Rev. B* **2003**, *68*, 165412.

(18) Todorova, M.; Li, W. X.; Ganduglia-Pirovano, M. V.; Stampfl, C.; Reuter, K.; Scheffler, M. *Phys. Rev. Lett.* **2002**, *89*, 096103.

(19) Michaelides, A.; Bocquet, M. L.; Sautet, P.; Alavi, A.; King, D. A. *Chem. Phys. Lett.* **2002**, *367*, 344.

(20) Michaelides, A.; Reuter, K.; Scheffler, M. *J. Vac. Sci. Technol. A* **2005**, *23*, 1487.

(21) Schnadt, J.; Michaelides, A.; Knudsen, J.; Vang, R. T.; Reuter, K.; Lægsgaard, E.; Scheffler, M.; Besenbacher, F. *Phys. Rev. Lett.* **2006**, *96*, 146101.

(22) Schmid, M.; Reicho, A.; Stierle, A.; Costina, I.; Klikovits, J.; Kostelnik, P.; Dubay, O.; Kresse, G.; Gustafson, J.; Lundgren, E.; Andersen, J. N.; Dosch, H.; Varga, P. *Phys. Rev. Lett.* **2006**, *96*, 146102.

(23) Reichelt, R.; Günther, S.; Rößler, M.; Wintterlin, J.; Kubias, B.; Jakobi, B.; Schlögl, R. *Phys. Chem. Chem. Phys.* **2007**, *9*, 3590.

(24) Reichelt, R.; Günther, S.; Wintterlin, J.; Moritz, W.; Aballe, L.; Mentes, T. O. *J. Chem. Phys.* **2007**, *127*, 134706.

(25) Klust, A.; Madix, R. J. *J. Chem. Phys.* **2007**, *126*, 084707.

(26) Xu, Y.; Greeley, J.; Mavrikakis, M. *J. Am. Chem. Soc.* **2005**, *127*, 12823.

(27) Greeley, J.; Mavrikakis, M. *J. Phys. Chem. C* **2007**, *111*, 7992.

(28) Reicho, A.; Stierle, A.; Costina, I.; Dosch, H. *Surf. Sci.* **2007**, *601*, L19.

(29) Linic, S.; Barteau, M. A. *J. Am. Chem. Soc.* **2002**, *124*, 310.

(30) Linic, S.; Barteau, M. A. *J. Am. Chem. Soc.* **2003**, *125*, 4034.

(31) Jones, G. S.; Mavrikakis, M.; Barteau, M. A.; Vohs, J. M. *J. Am. Chem. Soc.* **1998**, *120*, 3196.

(32) Bocquet, M. L.; Michaelides, A.; Loffreda, D.; Sautet, P.; Alavi, A.; King, D. A. *J. Am. Chem. Soc.* **2003**, *125*, 5620.

(33) Campell, C. T. *Surf. Sci.* **1985**, *157*, 43.

(34) Haruta, M. *Catal. Today* **1997**, *36*, 153.

(35) Valden, M.; Lai, X.; Goodman, D. W. *Science* **1998**, *281*, 1637.

(36) Hammer, B.; Hansen, L. B.; Nørskov, J. K. *Phys. Rev. B* **1999**, *59*, 7413.

(37) Perdew, J. P.; Chevary, J. A.; Vosko, S. H.; Jackson, K. A.; Pederson, M. R.; Singh, D. J.; Fiolhais, C. *Phys. Rev. B* **1992**, *46*, 6671.

(38) White, J. A.; Bird, D. M. *Phys. Rev. B* **1994**, *50*, 4954.

(39) Neugebauer, J.; Scheffler, M. *Phys. Rev. B* **1992**, *46*, 16067.

(40) Moruzzi, V. L.; Janak, J. F.; Schwarz, K. *Phys. Rev. B* **1988**, *37*, 790.

(41) Johnson, R. D., III., Ed.; NIST Computational Chemistry Comparison and Benchmark Database. *NIST Standard Reference Database*, 2004; Vol. Number 101, Release 10.

(42) Su, H. Y.; Bao, X. H.; Li, W. X. *J. Chem. Phys.* **2008**, *128*, 194707.

(43) Su, H. Y.; Yang, M. M.; Bao, X. H.; Li, W. X. *J. Phys. Chem. C* **2008**, *112*, 17303.

(44) Lundgren, E.; Gustafson, J.; Mikkelsen, A.; Andersen, J. N.; Stierle, A.; Dosch, H.; Todorova, M.; Rogal, J.; Reuter, K.; Scheffler, M. *Phys. Rev. Lett.* **2004**, *92*, 046101.

(45) Reuter, K.; Verónica Ganduglia-Pirovano, M.; Stampfl, C.; Scheffler, M. *Phys. Rev. B* **2002**, *65*, 165403.

(46) Gustafson, J.; Mikkelsen, A.; Borg, M.; Lundgren, E.; Köhler, L.; Kresse, G.; Schmid, M.; Varga, P.; Yuhara, J.; Torrelles, X.; Quirós, C.; Andersen, J. N. *Phys. Rev. Lett.* **2004**, *92*, 126102.

(47) Liu, Z. P.; Hu, P.; Alavi, A. *J. Am. Chem. Soc.* **2002**, *124*, 14770.

(48) Gong, X. Q.; Hu, P.; Raval, R. *J. Chem. Phys.* **2003**, *119*, 6324.

(49) Ojifinni, R. A.; Froemming, N. S.; Gong, J. L.; Pan, M.; Kim, T. S.; White, J. M.; Henkelman, G.; Mullins, C. B. *J. Am. Chem. Soc.* **2008**, *130*, 6801.

(50) Nolte, P.; Stierle, A.; Jin-Phillipp, N. Y.; Kasper, N.; Schulli, T. U.; Dosch, H. *Science* **2008**, *321*, 1654.

(51) Su, D. S.; Jacob, T.; Hansen, T. W.; Wang, D.; Schloegl, R.; Freitag, B.; Kujawa, S. *Angew. Chem., Int. Ed* **2008**, *47*, 1.

(52) Kokalj, A.; Gava, P.; Gironcoli, S.; Baroni, S. *J. Catal.* **2008**, *254*, 304.

(53) Christopher, P.; Linic, S. *J. Am. Chem. Soc.* **2008**, *130*, 11264.